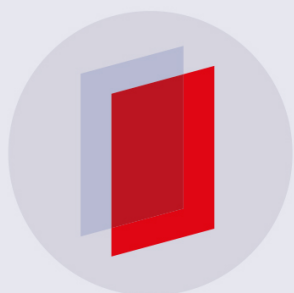


PAPER • OPEN ACCESS

## Sub-cycle attosecond control in frustrated double ionization of molecules

To cite this article: A Vilà *et al* 2019 *J. Phys. B: At. Mol. Opt. Phys.* **52** 015604

View the [article online](#) for updates and enhancements.



**IOP | ebooks™**

Bringing you innovative digital publishing with leading voices to create your essential collection of books in STEM research.

Start exploring the collection - download the first chapter of every title for free.

# Sub-cycle attosecond control in frustrated double ionization of molecules

A Vilà, G P Katsoulis<sup>1</sup> and A Emmanouilidou<sup>1</sup>

Department of Physics and Astronomy, University College London, Gower Street, London WC1E 6BT, United Kingdom

E-mail: [ucapaem@ucl.ac.uk](mailto:ucapaem@ucl.ac.uk)

Received 10 July 2018, revised 25 September 2018

Accepted for publication 12 November 2018

Published 11 December 2018



CrossMark

## Abstract

We demonstrate sub-cycle control of frustrated double ionization (FDI) of the two-electron triatomic molecule  $D_3^+$  when driven by two orthogonally polarized two-color laser fields, where a weak mid-infrared laser field is employed to probe the FDI process triggered by a strong near-infrared laser field. We use a three-dimensional semi-classical model that fully accounts for the electron and nuclear motion in strong fields. We analyze the FDI probability and the distribution of the momentum of the escaping electron along the polarization direction of the mid-infrared laser field. These observables when considered in conjunction bear clear signatures of sub-cycle control of FDI. We find that the momentum distribution of the escaping electron has a striking hive-shape with features that can accurately be mapped to the time that one of the two electrons tunnel-ionizes at the start of the break-up process. This mapping distinguishes consecutive tunnel-ionization times within a cycle of the mid-infrared laser field but not tunnel-ionization times differing by an integer number of cycles.

Keywords: frustrated ionization, molecules driven by strong fields, ultrafast processes

(Some figures may appear in colour only in the online journal)

## 1. Introduction

Accounting for roughly 10% of all ionization events, frustrated double ionization (FDI) is one of the major processes when multi-center molecules are driven by intense laser fields [1, 2]. In frustrated ionization an electron first tunnel-ionizes in the driving laser field. Then, due to the electric field of the laser pulse, it is recaptured by the parent ion in a Rydberg state [3]. In FDI an electron escapes and another one occupies a Rydberg state at the end of the laser pulse. A number of experimental studies in the context of  $H_2$  [1] and of the triatomic molecules  $D_3^+$  and  $H_3^+$  have addressed FDI over the last few years [4–6]. Two pathways were identified to underlie FDI in previous theoretical studies of strongly-driven two-electron diatomic and triatomic molecules [2, 7]. Electron–electron correlation is important, primarily, for one of the two pathways.

Very recently, we proposed a scheme to identify the important role of electron–electron correlation in FDI in future experiments [8] using orthogonally polarized two-color laser fields (OTC). Two-color laser fields have been efficiently employed to control electron motion [9, 10] and to steer the outcome of chemical reactions [11–13]. The field-free orientation of molecules [14–16], the generation of high-harmonic spectra [17–20], probing atomic and molecular orbital symmetry [21–23] and controlling double ionization in atoms [24–29] are some of the other applications of two-color laser fields. Moreover, in a recent experiment [30] it was shown that a weak mid-IR pulse acts as a streak camera that time-resolves the strong-field dynamics of the escaping electron in single ionization triggered by a near-IR pulse in atoms. In [8] we have shown how to control the pathway of FDI where electron–electron correlation is important by employing a triggering 800 nm near-infrared (near-IR) strong laser field and a probing 400 nm weaker laser field. We showed that, together, the FDI probability and the V-shape of the momentum of the escaping electron along the 800 nm laser field bear clear signatures of the turning on and off of electron–electron correlation in FDI.

<sup>1</sup> Author to whom any correspondence should be addressed.

Here, we demonstrate in addition sub-cycle attosecond control in FDI of triatomic molecules by employing OTC laser fields where a weak mid-IR 2400 nm laser field is used as the probing field. We show that the FDI probability changes significantly as a function of the time delay between the triggering 800 nm strong laser field and the probing one. The change is mainly due to the FDI pathway where electron–electron correlation is important. Interestingly, we find that the momentum distribution of the escaping electron along the mid-IR laser field has a striking hive-shape. We find a one-to-one correspondence between the features of this hive-shape and the time that one of the two electrons tunnel-ionizes at the start of the break-up process of the strongly-driven molecule. These tunnel-ionization times take place around the extrema of the near-IR laser field, since the mid-IR pulse is weak. Hence, this mapping allows us to identify the traces that each of the six tunnel-ionization times in one cycle of the mid-IR pulse imprint on the hive-shape. We are thus demonstrating sub-cycle control, since we are resolving the different tunneling times in one cycle of the near-IR laser field using a mid-IR laser field as a probe. Moreover, as we show, the resulting hive-shape undergoes changes in less than roughly 1/4 of the period of the near-IR laser field (2.7 fs) demonstrating attosecond control. To achieve sub-cycle control the frequency of the probing field must be smaller than the frequency of the near-IR field. However, as we later show in the results section a smaller frequency of the probing field results in a smaller FDI probability. Hence, our choice of wavelength for the probe laser field is such that while sub-cycle control is achieved the FDI probability is large enough to be experimentally accessible.

Treating two electrons and three-nuclei in a strong laser field is a challenge for fully *ab-initio* quantum mechanical calculations. The latter methods can currently address one electron triatomic molecules [31]. Therefore, classical and semi-classical models are essential for understanding the fragmentation of strongly-driven triatomic molecules [7, 32]. We previously employed a three-dimensional (3D) semi-classical model that provided significant insights into FDI for strongly-driven  $\text{H}_2$  [2] and  $\text{D}_3^+$  [7]. For instance, a result we previously obtained with this model was the distribution of the kinetic energy release of the Coulomb exploding nuclei in FDI of  $\text{D}_3^+$  which was in good agreement with experimental results [6]. We use the same model in our current studies.

## 2. Method

The OTC laser field we employ consists of an 800 nm laser field, i.e.  $\omega_1 = 0.057$  a.u. with field strength of  $E_{\omega_1}$  equal to 0.08 a.u. and a weak 2400 nm laser field, i.e.  $\omega_2 = \omega_1/3$ , with field strength  $E_{\omega_2}$  equal to 0.0253 a.u.. The intensity of the mid-IR field is taken to be one tenth of the intensity of the near-IR field. The ponderomotive energies,  $E_{\omega}^2/4\omega^2$ , of the near-IR and mid-IR laser fields are equal to 0.49 a.u. and 0.44 a.u. respectively, and are thus comparable. In contrast, in our previous study with OTC fields [8] we employed a probing field of 400 nm with ponderomotive energy much

smaller than the one of the 800 nm pulse. The combined laser field is given by

$$\begin{aligned} \mathbf{E}(t, \Delta t) &= E_{\omega_1} f(t) \cos(\omega_1 t) \hat{z} \\ &+ E_{\omega_2} f(t - \Delta t) \cos(\omega_2(t - \Delta t)) \hat{x} \\ f(t) &= \exp\left(-2 \ln 2 \left(\frac{t}{\tau}\right)^2\right), \end{aligned} \quad (1)$$

where  $\tau = 40$  fs is the full-width-half-maximum duration of the OTC laser field.

Here, we employ an initial state for  $\text{D}_3^+$  that is a superposition of equilateral triangular-configuration vibrational states  $\nu = 1 - 12$  [4, 6]. The reason for our choice is that this state is accessed experimentally via the reaction  $\text{D}_2 + \text{D}_2^+ \rightarrow \text{D}_3^+ + \text{D}$ . The outer classical turning point of the vibrational levels [33, 34] changes from 2.04 a.u. ( $\nu = 1$ ) to 2.92 a.u. ( $\nu = 12$ ) [35, 36]. In our model we assume that most of the ionization of  $\text{D}_3^+$  occurs at the outer turning point. Moreover, for all vibrational levels, we consider the nuclei to be initially at rest, since we have found that the ionization dynamics does not depend significantly on their initial state [37].

Our 3D model involves two quantum-mechanical aspects. One aspect refers to the first step in our model where we take one electron (electron 1) to tunnel-ionize at time  $t_0$  in the field-lowered Coulomb barrier since the combined strength of the two laser fields is within the below-the-barrier ionization regime. We use a semi-classical formula [38] to compute the ionization rate in this step. We select  $t_0$  using importance sampling [39] in the time interval the two-color laser field is present. The ionization rate is then used as the importance sampling distribution. The component of the velocity of electron 1 that is parallel to the total OTC laser field is set equal to zero while the transverse one is given by a Gaussian [40, 41]. For the electron that is initially bound (electron 2) the initial state is described by a microcanonical distribution [42].

The other quantum mechanical aspect of our 3D model is essential in order to accurately account for the enhanced ionization (EI) process [43, 44]. Namely, we allow for each electron to tunnel during the propagation with a probability given by the Wentzel–Kramers–Brillouin approximation [2, 37]. We note that in the EI process at a critical distance of the nuclei, a double potential well is formed such that it is easier for an electron bound to the higher potential well to tunnel to the lower potential well and subsequently ionize. The time propagation starts at time  $t_0$  and is determined by the Hamiltonian of the strongly-driven five-body system. It is important to note that we fully account for the Coulomb singularities during the time propagation [37].

After propagating the trajectories to the asymptotic time limit, we record the events of FDI of  $\text{D}_3^+$ . For these events the final fragments are a neutral excited fragment  $\text{D}^*$ , two  $\text{D}^+$  ions and one escaping electron. In the neutral excited fragment  $\text{D}^*$  the electron occupies an excited (Rydberg) state with quantum number  $n > 1$ . Here, as in our previous studies [2, 7, 37], we record two pathways of FDI. In pathway A, electron 1 tunnel-ionizes and escapes early on. Electron 2 gains energy from the laser field in an EI-like process and

tunnel-ionizes. When the laser field is turned off, electron 1 does not have enough drift energy to escape and eventually occupies a Rydberg state,  $D^*$ . In pathway B, electron 1 tunnel-ionizes and quivers in the laser field and eventually returns to the core. Electron 2 gains energy both from the laser field in an EI-like process as well as from the returning electron 1. Electron 2 eventually tunnel-ionizes after a few periods of the laser field. The main difference between pathway A and B is that, once the laser field is turned on, the electron that finally ionizes does so much faster in pathway A than in pathway B.

In many experimental studies, strongly-driven molecules are randomly oriented with respect to the laser field. However, due to the challenging computations involved in obtaining the FDI probability we consider only two cases of planar alignment, that is, one side of the equilateral, molecular triangle is either parallel or perpendicular to the  $\hat{z}$ -component of the laser field. Moreover, we only compute the FDI probability for the  $\nu = 8$  state of  $D_3^+$ , see also [8]. This is a good approximation, since we find that the  $\nu = 6, 7, 8, 9$  states contribute the most in the sum in equation (2). We find that the FDI probabilities and the distributions of the momentum of the escaping electron are very similar for all these states. We compute the FDI probability as a function of the time delay  $\Delta t$  of the  $\omega - \omega/3$  laser pulses using

$$P^{\text{FDI}}(\Delta t) = \frac{\sum_i P_i \Gamma(\Delta t, \nu, i) P^{\text{FDI}}(\Delta t, \nu, i)}{\sum_i P_i \Gamma(\Delta t, \nu, i)}, \quad (2)$$

where  $i$  refers to the different orientations of the molecule with respect to the  $z$ -axis and  $\nu = 8$ .  $\Gamma(\Delta t, \nu, i)$  is given by

$$\Gamma(\Delta t, \nu, i) = \int_{t_i}^{t_f} \Gamma(t_0, \Delta t, \nu, i) dt_0, \quad (3)$$

where we integrate over the duration of the OTC field.  $\Gamma(t_0, \Delta t, \nu, i)$  is the ionization rate at time  $t_0$  for a certain molecular orientation  $i$ , vibrational state  $\nu$  and time delay  $\Delta t$ .  $P_i$  is the percentage of the vibrational state  $\nu = 8$  in the initial state of  $D_3^+$  [35].  $P^{\text{FDI}}(\Delta t, \nu, i)$  is the number of FDI events out of all initiated classical trajectories for a certain molecular orientation  $i$ , the vibrational state  $\nu = 8$  and time delay  $\Delta t$ .

### 3. Results and discussion

In figure 1, we plot the probability of FDI and of pathway A and B as a function of the time delay between the mid-IR and the near-IR laser pulses. The time delay,  $\Delta t$ , is expressed in units of the period of the near-IR laser field  $T_{\omega_1}$ . We consider  $\Delta t$  in one cycle of the mid-IR laser field that corresponds to three cycles of the near-IR laser pulse, i.e.  $\Delta t \in [-1.5, 1.5)T_{\omega_1}$ . We find that the FDI probability changes as a function of the time delay. We find that pathway B with a probability that varies significantly from 2.6% to 0% is the main reason for the change in the FDI probability. In contrast, the probability of pathway A only varies from 1.1% to 0.77%. In the absence of the mid-IR laser field the probability of pathway A and B is 3.6% and 4.9%, respectively. Thus, the probing mid-IR laser field decreases the maximum value of the FDI probability from 8.5% to 3.7%. This was not

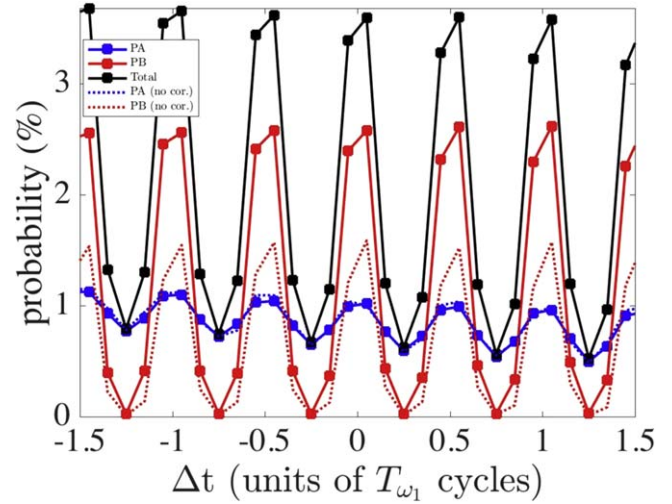


**Figure 1.** (a) FDI probability and probability of pathway A and B as a function of the time delay with electron–electron correlation turned on (solid lines) and off (dotted lines).

the case in our previous study where we found that the probing 400 nm laser pulse did not affect the maximum value of the FDI probability [8]. We explain later in this section why this is the case.

A consequence of the large ponderomotive energy of the mid-IR laser pulse is that the values of the extrema of the probability of FDI and of pathway A and B decrease with increasing values of  $\Delta t$  in the time interval  $[-1.5, 1.5)T_{\omega_1}$ , see figure 1. We find that the values of the extrema of the FDI probabilities are larger for negative rather than positive time delays. Electron 1 tunnel-ionizes mostly from the extrema around the peak intensity of the near-IR laser field. For negative time delays, the atom encounters first the peak of the mid-IR and then the peak of the near-IR laser pulse. Therefore, for negative (positive) time delays when electron 1 tunnel-ionizes it mostly encounters a decreasing (increasing) force from the mid-IR laser field along the  $\hat{x}$ -axis. This force results in electrons moving away from the nuclei and thus decreases the FDI probabilities. Since the force from the mid-IR laser pulse is less for negative time delays, it follows that the FDI probabilities decrease less in this case.

Electron–electron correlation plays a significant role for pathway B of FDI [2, 8]. Indeed, by turning off the electron–electron correlation in our computations, we find that the probability of pathway A as a function of the time delay is the same as when the electron–electron correlation is turned on, see figure 1. However, when electron–electron correlation is turned off the maximum value of the probability of pathway B reduces to only half its value compared to when electron–electron correlation is on.

In figure 2(a1), we plot the distribution of the momentum  $p_x$  of the escaping electron for FDI along the mid-IR laser field as a function of  $\Delta t$  in the time interval  $[-1.5, 1.5)T_{\omega_1}$  in steps of  $\Delta t = 0.1T_{\omega_1}$ . We find that the distribution of  $p_x$  has a hive-shape. This hive-shape is mainly due to pathway A, see figure 2(a2). To understand the shape of  $p_x$  for pathway A, we first investigate the time electron 1 tunnel-ionizes as a

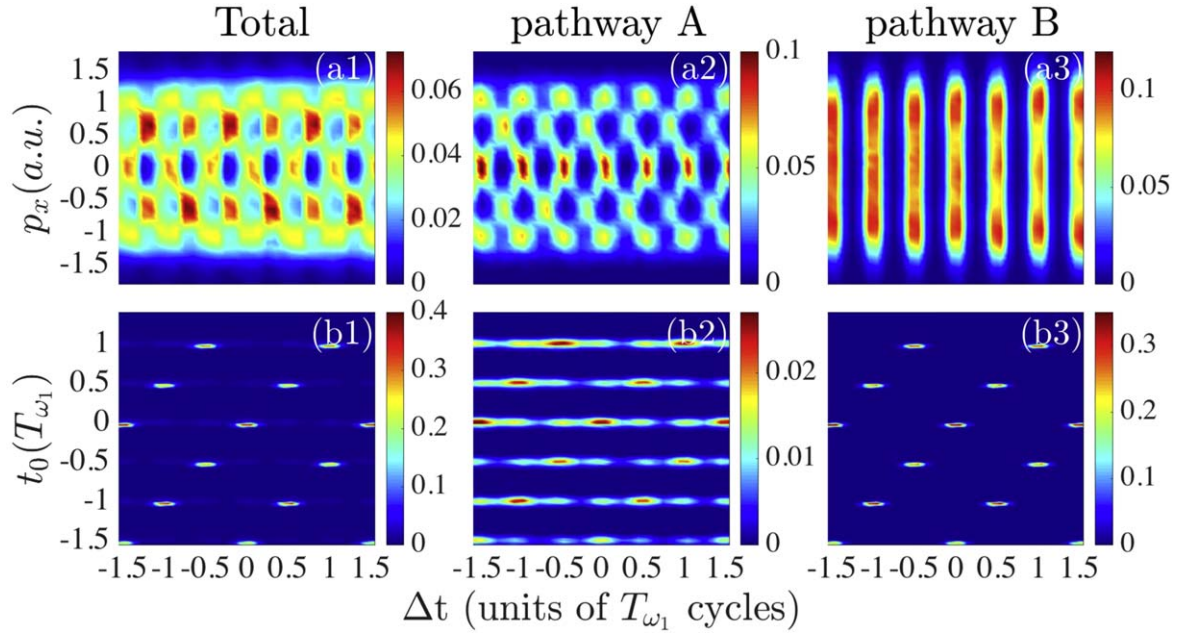


**Figure 2.** The distribution of  $p_x$  for FDI (a1) and for pathways A (a2) and B (a3) are plotted as a function of  $\Delta t$ . For each  $\Delta t$ , the distribution of  $p_x$  in (a2)–(a3) is normalized with respect to the total FDI probability, while in (a1) it is normalized to 1. The distribution of the time electron 1 tunnel-ionizes for FDI (b1) and for pathways A (b2) and B (b3) is plotted as a function of  $\Delta t$ . For each  $\Delta t$ , the distribution of  $t_0$  in (b1)–(b3) is normalized with respect to the total FDI probability.

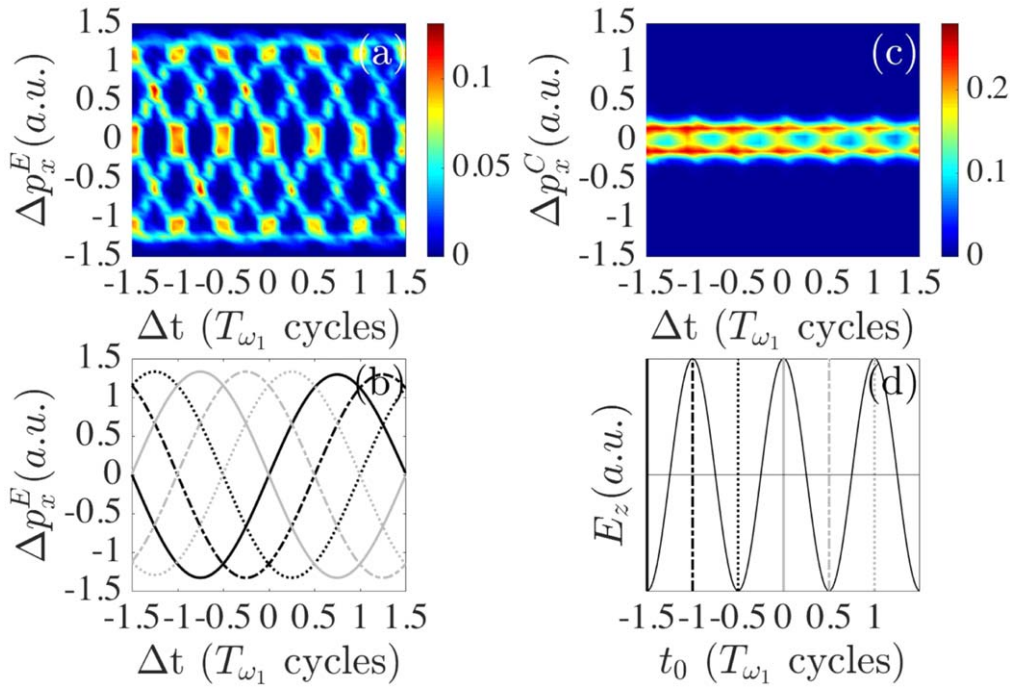


**Figure 3.** The distributions of  $\Delta p_x^E$  (a) and  $\Delta p_x^C$  (c) for pathway A are plotted as a function of  $\Delta t$ . For each  $\Delta t$  the distributions in (a) and (c) are normalized to the probability for pathway A. (b)  $\Delta p_x^E$  is plotted as a function of  $\Delta t$  for the six  $t_0$ s corresponding to extrema of  $E_{\omega_1}$  within one cycle of the 2400 nm laser field, which are shown in (d).

function of  $\Delta t$ , see figure 2(b2). When the mid-IR laser field is turned off  $t_0$  is centered around the extrema of the near-IR laser field. For one cycle of the mid-IR laser field electron 1 tunnel-ionizes from six extrema of the near-IR laser field, see figure 3(d). We find that when the mid-IR laser field is turned on electron 1 in pathway A still tunnel-ionizes from the  $t_0$ s

corresponding to these six extrema. However, for each  $\Delta t$  we find that electron 1 tunnel-ionizes in each half-cycle of the near-IR laser pulse at the  $t_0$  which coincides with the time  $t_{\max}$  when the combined OTC laser field in equation (1) is maximum, see figure 2(b2). This is expected since when electron 1 is the escaping electron the time electron 1 tunnel-ionizes

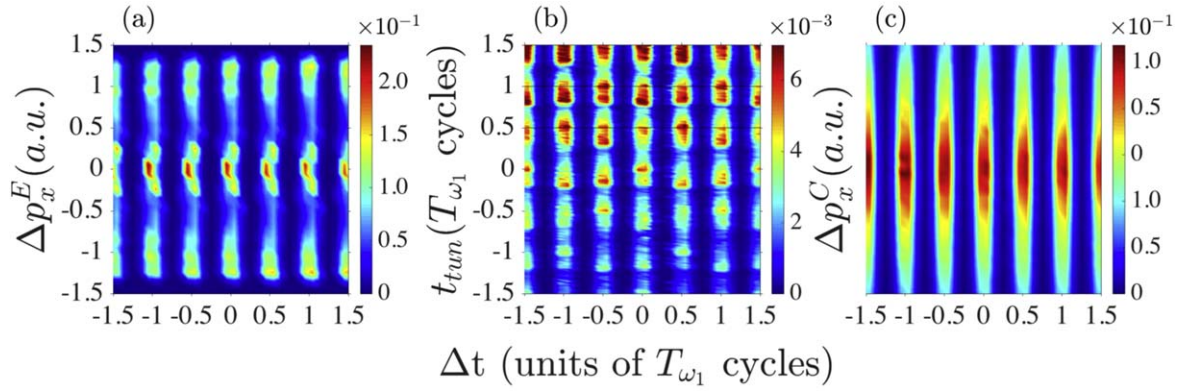


**Figure 4.** The distributions of  $\Delta p_x^E$  (a), the time that electron 2 tunnel-ionizes during the time propagation,  $t_{\text{tun}}$ , (b) and  $\Delta p_x^C$  (c) for pathway B are plotted as a function of  $\Delta t$ . For each  $\Delta t$  the distributions in (a)–(c) are normalized to the probability for pathway B.

will be roughly equal with the time the ionization rate is maximum. This is not the case for pathway B. At  $\Delta t = (n + 1/4)T_{\omega_1}/2$  the probability of pathway B is zero. Around  $\Delta t = nT_{\omega_1}/2$ , where the probability of pathway B is maximum, electron 1 tunnel-ionizes only from two out of the six  $t_0$ s, see figure 2(b2). We explain later why this is the case.

To understand the hive-shape in the distribution of  $p_x$  for pathway A, we consider separately the contribution of the mid-IR laser field and of the core to the final momentum  $p_x$ , with  $p_x = \Delta p_x^E + \Delta p_x^C + p_{x,t_i}$ .  $\Delta p_x^C$  is the momentum change due to the core as well as the electron–electron interaction. We find the contribution of the electron–electron interaction to  $\Delta p_x^C$  to be very small.  $p_{x,t_i}$  is the distribution of the  $x$ -component of the momentum of the escaping electron at time  $t_i$ . For pathway A  $t_i$  is the time that electron 1 tunnel-ionizes,  $t_0$ . We find that  $p_{x,t_0}$  has only a small contribution to  $p_x$ . The momentum change from the mid-IR laser field and the core are given by

$$\begin{aligned} \Delta p_x^E(\Delta t, t_i) &= \int_{t_i}^{\infty} -E_{\omega_2}(t) dt, \\ \Delta p_x^C(\Delta t, t_i) &= \int_{t_i}^{\infty} \left( \sum_{i=1}^3 \frac{\mathbf{R}_i - \mathbf{r}_1}{|\mathbf{r}_1 - \mathbf{R}_i|^3} + \frac{\mathbf{r}_1 - \mathbf{r}_2}{|\mathbf{r}_1 - \mathbf{r}_2|^3} \right) \cdot \hat{x} dt. \end{aligned} \quad (4)$$

In figure 3(c) we plot  $\Delta p_x^C$  as a function of the time delay.  $\Delta p_x^C$  has a two-band structure that is symmetric with respect to  $p_x$  equal to zero. We find that the upper (lower) band corresponds mostly to pathway A events where electron 1 tunnel-ionizes from the negative (positive)  $\hat{x}$ -axis.

Figure 3(a), clearly shows that the hive-shape of the distribution  $p_x$  is accounted for by the momentum change due to the mid-IR laser field. Indeed, in figure 3(b), we reproduce the outline of the hive-shape of  $p_x$  in figure 3(a)—the result of our full scale computations—by employing a very simple model. Specifically, using equation (1), we compute  $\Delta p_x^E$  as a function of  $\Delta t$  for each of the six  $t_0$ s electron 1 tunnel-ionizes from (figure 3(d)). Figure 3(b) clearly shows how the  $\cos/\sin$  like curves of  $\Delta p_x^E$  as a function of  $\Delta t$  for each of the six  $t_0$ s within one cycle of the mid-IR laser field intertwine to result in the hive-shape of  $p_x$  for pathway A. Hence, we have established a one-to-one correspondence, i.e. mapping,

between the features of the hive-shape in figures 3(a) and 2(a2) and the  $t_0$ s electron 1 tunnel-ionizes from within one cycle of the mid-IR laser pulse. That is, the 2400 nm laser pulse, probes the momentum  $p_x$  that corresponds to different  $t_0$ s. This mapping distinguishes between different  $t_0$ s within one cycle of the mid-IR laser field but does not distinguish between  $t_0$ s that differ by an integer number of cycles of the mid-IR field.

We next focus on the contribution of pathway B to the distribution of  $p_x$ , see figure 2(a3). First, we explain why the probability of pathway B is zero at  $\Delta t = (n + 1/4)T_{\omega_1}/2$ . It is enough to use the six  $t_0$ s at the extrema of the near-IR laser field in the interval  $[-1.5, 1.5] T_{\omega_1}$  where electron 1 tunnel-ionizes. Figure 3(b) shows that  $\Delta p_x^E$  is not zero for all six  $t_0$ s at  $\Delta t = (n + 1/4)T_{\omega_1}/2$ . Hence, at these  $\Delta t$ s the non zero momentum change from the mid-IR laser field pushes electron 1 away from the core along the  $\hat{x}$ -axis. As a result, electron 1 does not return to the core to ionize electron 2 and the probability of pathway B is zero. On the other hand, at  $\Delta t = nT_{\omega_1}/2$ , figure 3(b) shows that there are two  $t_0$ s where  $\Delta p_x^E = 0$ . As a result, electron 1 can return to the core and ionize electron 2 and the probability of pathway B is non zero. This is consistent with figure 2(b3), which clearly shows that at  $\Delta t = nT_{\omega_1}/2$ , two  $t_0$ s contribute to the tunnel-ionization times of electron 1 while for all other  $t_0$ s no  $t_0$  contributes.

In figure 4(c) we plot the momentum change along the mid-IR laser field due to the core plus the electron–electron repulsion, respectively. To compute these contributions, we employ equation (4) using as  $t_i$  the time  $t_{\text{tun}}$ . The latter is the time electron 2 tunnel-ionizes during the time propagation. Unlike pathway A, the contribution of the core for pathway B is broad at the  $t$ s where the probability of pathway B is not zero, see figure 4(c). This is consistent with electron 2 being the escaping electron in pathway B. Electron 2 has more time to interact with the nucleus before it tunnel-ionizes and finally escapes giving rise to a broad distribution  $p_x$ .

Figure 4(a) shows that the momentum change of electron 2 from the mid-IR laser field is similar to  $p_x$  for pathway A for the  $t$ s where the probability of pathway B is not zero. Indeed,

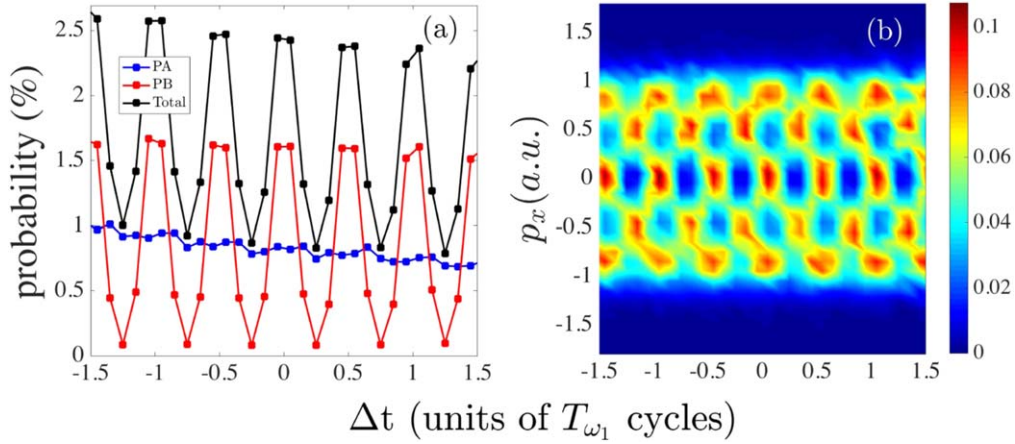


Figure 5. (a) And (b) the same as figures 1 and 2(a1), respectively, for  $H_2$ .

for pathway A the  $\Delta p_x^E$  of electron 1 from the six  $t_0$ s in the time interval  $t_0 \in [-1.5, 1.5]T_{\omega_1}$  give rise to the hive-shape of the distribution  $p_x$ . This is also the case for pathway B, however, the relevant  $t_i$  time in equation (4) is not  $t_0$  but the time  $t_{\text{tun}}$  electron 2 tunnel-ionizes during the time propagation. We show in figure 4(b) that electron 2 tunnel-ionizes around the extrema of the near-IR laser field. Therefore, a hive-shape for  $p_x$  of electron 2 is obtained for pathway B as for pathway A. The main difference is that pathway B is zero at  $\Delta t = (n + 1/4)T_{\omega_1}/2$ . Another difference is that since  $t_{\text{tun}}$  is more broadly distributed than  $t_0$  around the extrema of the near-IR laser field the hive-shape is more broad at  $\Delta t = nT_{\omega_1}/2$  for pathway B than A, compare figure 4(a) with figure 3(a). Thus,  $p_x$  for pathway B further enhances the hive-shape of the total FDI distribution  $p_x$  at  $\Delta t = nT_{\omega_1}/2$ .

We now explain the reason why the FDI probability for  $D_3^+$  when driven by an 800 nm pump laser field reduces less when we employ a probing laser field of 400 nm [8] compared to a 2400 nm one. The momentum change  $\Delta p_x^E$  of either electron due to the laser field along the  $\hat{x}$ -axis is proportional to  $E_{\omega_2}/\omega_2 \sin(\omega_2(t_i - \Delta t))$ , assuming  $f(t) = 1$  in equation (1). For pathway B, substituting for  $\omega_2 = \omega_1/3$  for the 2400 nm laser field and  $2\omega_1$  for the 400 nm one and using  $t_i = t_0 = n\pi/\omega_1$ , with  $n$  an integer, we find that the momentum change of electron 1 is proportional to  $E_{\omega_2}/\omega_2 \sin(\omega_1/3(n\pi/\omega_1 - \Delta t))$  and  $E_{\omega_2}/\omega_2 \sin(2\omega_1 \Delta t)$ , respectively. Thus, for the mid-IR probing field the momentum change depends on the time electron 1 tunnel-ionizes, while for the 400 nm laser field it does not. The FDI probability for pathway B is maximum when this momentum change of electron 1 is zero. This condition is satisfied for all  $t_0$ s for the 400 nm laser field but only for two  $t_0$ s out of six consecutive  $t_0$ s for the 2400 nm one, as we have already discussed in figure 3(b). It follows that electron 1 returns for a smaller number of  $t_0$ s to re-collide with the core and thus transfer energy to electron 1 for the 2400 nm laser field. Therefore, the FDI probability for pathway B is smaller for a 2400 nm probing field than a 400 nm one. For pathway A, the momentum change of electron 2 at time  $t_{\text{tun}}$  when electron 2 tunnel-ionizes is again given by the same formulas as above;  $t_i = t_{\text{tun}}$  and  $t_{\text{tun}}$  is still centered around the extrema of the

near-IR laser field. As a result, for the 2400 nm laser field, electron 2 gains momentum different than zero for a minimum of four and up to six  $t_{\text{tun}}$ s out of the six consecutive  $t_{\text{tun}}$ s as a function of the  $\Delta t$ , see figure 3(b). For the 400 nm field, the momentum gain of electron 2 is independent of  $t_{\text{tun}}$ . Thus, the momentum gain is different than zero for more values of  $t_{\text{tun}}$  for the 400 nm compared to the 2400 nm laser field. However,  $E_{\omega_2}/\omega_2$  is three times larger for the parameters we use in the current study where we employ a 2400 nm laser field than for the parameters in our previous study [8] where we employ a 400 nm one. Hence, the overall momentum gain is larger for the 2400 nm laser field leading to the more probable escape of electron 2 and consequently to a smaller FDI probability. Moreover, given the dependence of the electron momentum gain on the tunnel-ionization time for the 2400 nm laser field but not for the 400 nm one, it should now be clear that while the 2400 nm laser field is appropriate for sub-cycle control the 400 nm one is not.

Finally, we show that sub-cycle attosecond control can also be achieved with OTC fields for  $H_2$ . We choose  $E_{\omega_1} = 0.064$  a.u. so that  $E_{\omega_1}$  for  $H_2$  and  $D_3^+$  has the same percentage difference from the field strength that corresponds to over-the-barrier ionization. We choose  $E_{\omega_2}$  to be such that the intensity of the  $E_{\omega_2}$  laser field is one tenth of the intensity corresponding to the  $E_{\omega_1}$  laser field, as for the  $D_3^+$  molecule. We show in figure 5(a) that the FDI probability changes from a maximum value of 2.7% to a minimum of 1% as a function of the time delay between the two pulses. The probability of pathway A remains almost constant varying from 1% to 0.9%. However, the probability of pathway B changes from 1.7% to 0.1% and accounts for the change in the FDI probability. We note that in figure 5 we only consider the orientation where the inter-nuclear axis is parallel to the 800 nm laser field since for the perpendicular orientation the probability is zero. Therefore, the FDI probability averaged over all molecular orientations will be smaller than the values presented in figure 5(a) and thus from the FDI probability for  $D_3^+$ . Smaller FDI probability aside, figure 5(b) shows that a similar hive-shape of the momentum distribution of the escaping electron for FDI as a function of  $\Delta t$  is obtained for  $H_2$  and  $D_3^+$  alike.

## 4. Conclusions

In conclusion, we have shown that sub-cycle attosecond control for the FDI process can be achieved with OTC laser fields in  $D_3^+$ , using a mid-IR laser field as the probing one. We employ a near-IR laser field that triggers the FDI process and a weak mid-IR laser field to probe and control the FDI process. We find that the FDI probability changes sharply with the time delay between the two laser fields. Moreover, we identify a hive-shape in the momentum distribution of the escaping electron in FDI along the mid-IR laser field. We show that different features of this hive-shape of the electron momentum distribution can be mapped back to electron 1 tunnel-ionizing from six consecutive extrema of the near-IR laser field within one cycle of the mid-IR laser field. Moreover, we have shown that tunnel-ionization of electron 1 from only two of the six extrema of the near-IR laser field contributes to pathway B of FDI. Future studies could explore the effect of interference in the hive-shape of the momentum of the escaping electron.

## Acknowledgments

A E acknowledges the EPSRC grant no. N031326 and the use of the computational resources of Legion at UCL.

## ORCID iDs

G P Katsoulis  <https://orcid.org/0000-0002-1211-3841>

A Emmanouilidou  <https://orcid.org/0000-0002-6255-9622>

## References

- [1] Manschwetus B, Nubbemeyer T, Gorling K, Steinmeyer G, Eichmann U, Rottke H and Sandner W 2009 *Phys. Rev. Lett.* **102** 113002
- [2] Emmanouilidou A, Lazarou C, Staudte A and Eichmann U 2012 *Phys. Rev. A* **85** 011402(R)
- [3] Nubbemeyer T, Gorling K, Saenz A, Eichmann U and Sandner W 2008 *Phys. Rev. Lett.* **101** 233001
- [4] McKenna J, Sayler A M, Gaire B, Johnson N G, Carnes K D, Esry B D and Ben-Itzhak I 2009 *Phys. Rev. Lett.* **103** 103004
- [5] Sayler A M, McKenna J, Gaire B, Kling N G, Carnes K D and Ben-Itzhak I 2012 *Phys. Rev. A* **86** 033425
- [6] McKenna J, Sayler A M, Gaire B, Kling N G, Esry B D, Carnes K D and Ben-Itzhak I 2012 *New J. Phys.* **14** 103029
- [7] Chen A, Price H, Staudte A and Emmanouilidou A 2016 *Phys. Rev. A* **94** 043408
- [8] Chen A, Kling M and Emmanouilidou A 2017 *Phys. Rev. A* **96** 033404
- [9] Kitzler M and Lezius M 2005 *Phys. Rev. Lett.* **95** 253001
- [10] Richter M, Kunitski M, Schöffler M, Jahnke T, Schmidt L P H and Dörner R 2016 *Phys. Rev. A* **94** 033416
- [11] Ray D et al 2009 *Phys. Rev. Lett.* **103** 223201
- [12] Li H, Ray D, De S, Znakovskaya I, Cao W, Laurent G, Wang Z, Kling M F, Le A T and Cocke C L 2011 *Phys. Rev. A* **84** 043429
- [13] Gong X, He P, Song Q, Ji Q, Pan H, Ding J, He F, Zeng H and Wu J 2014 *Phys. Rev. Lett.* **113** 203001
- [14] De S et al 2009 *Phys. Rev. Lett.* **103** 153002
- [15] Frumker E, Hebeisen C T, Kajumba N, Bertrand J B, Wörner H J, Spanner M, Villeneuve D M, Naumov A and Corkum P B 2012 *Phys. Rev. Lett.* **109** 113901
- [16] Znakovskaya I, Spanner M, De S, Li H, Ray D, Corkum P, Litvinyuk I V, Cocke C L and Kling M F 2014 *Phys. Rev. Lett.* **112** 113005
- [17] Kim I J, Kim C M, Kim H T, Lee G H, Lee Y S, Park J Y, Cho D J and Nam C H 2005 *Phys. Rev. Lett.* **94** 243901
- [18] Kitzler M, Xie X, Roither S, Scrinzi A and Baltuška A 2008 *New J. Phys.* **10** 025029
- [19] Brugnera L et al 2010 *Opt. Lett.* **35** 3994
- [20] Brugnera L, Hoffmann D J, Siegel T, Frank F, Zaïr A, Tisch J W G and Marangos J P 2011 *Phys. Rev. Lett.* **107** 153902
- [21] Dudovich N, Smirnova O, Levesque J, Mairesse Y, Ivanov M Y, Villeneuve D M and Corkum P B 2006 *Nat. Phys.* **2** 781
- [22] Niikura H, Dudovich N, Villeneuve D M and Corkum P B 2010 *Phys. Rev. Lett.* **105** 053003
- [23] Shafir D, Mairesse Y, Villeneuve D M, Corkum P B and Dudovich N 2009 *Nat. Phys.* **5** 412
- [24] Zhou Y, Liao Q, Zhang Q, Hong W and Lu P 2010 *Opt. Express* **18** 632
- [25] Zhou Y, Huang C, Tong A, Liao Q and Lu P 2011 *Opt. Express* **19** 2301
- [26] Chen L, Zhou Y, Huang C, Zhang Q and Lu P 2013 *Phys. Rev. A* **88** 043425
- [27] Zhang L et al 2014 *Phys. Rev. Lett.* **112** 193002
- [28] Mancuso C A et al 2016 *Phys. Rev. Lett.* **117** 133201
- [29] Eckart S et al 2016 *Phys. Rev. Lett.* **117** 133202
- [30] Kübel M et al 2018 *Phys. Rev. Lett.* **119** 183201
- [31] Lefebvre C, Lu H Z, Chelkowski S and Bandrauk A D 2014 *Phys. Rev. A* **89** 023403
- [32] Lötstedt E, Kato T and Yamanouchi K 2011 *Phys. Rev. Lett.* **106** 203001
- [33] Ergler T, Feuerstein B, Rudenko A, Zrost K, Schröter C D, Moshhammer R and Ullrich J 2006 *Phys. Rev. Lett.* **97** 103004
- [34] Goll E, Wunner G and Saenz A 2006 *Phys. Rev. Lett.* **97** 103003
- [35] Anicich V G and Futrell J H 1984 *Int. J. Mass Spectrom. Ion Process.* **55** 189
- [36] Talbi D and Saxon R P 1988 *J. Chem. Phys.* **89** 2235
- [37] Price H, Lazarou C and Emmanouilidou A 2014 *Phys. Rev. A* **90** 053419
- [38] Murray R, Spanner M, Patchkovskii S and Ivanov M Y 2011 *Phys. Rev. Lett.* **106** 173001
- [39] Rubinstein R Y and Froese D P 2007 *Simulation and the Monte Carlo Method* 2nd edn (New York: Wiley)
- [40] Ammosov M V, Delone N B and Krainov V P 1986 *Sov. Phys. - JETP* **64** 1191
- [41] Popov V S 2004 *Phys.-Usp.* **47** 855
- [42] Chen A, Lazarou C, Price H and Emmanouilidou A 2016 *J. Phys. B* **49** 235001
- [43] Niikura H, Légaré F, Hasbani R, Bandrauk A D, Ivanov M Y, Villeneuve D M and Corkum P B 2002 *Nature* **417** 917
- [44] Zuo T and Bandrauk A D 1995 *Phys. Rev. A* **52** R2511(R)
- Seideman T, Ivanov M Y and Corkum P B 1995 *Phys. Rev. Lett.* **75** 2819
- Villeneuve D M, Ivanov M Y and Corkum P B 1996 *Phys. Rev. A* **54** 736
- Dehghanian E, Bandrauk A D and Kamta G L 2010 *Phys. Rev. A* **81** 061403(R)